ADVANCED ENERGY MATERIALS
www.advenergymat.de

Characterization of Polysulfide Radicals Present in an Ether-Based Electrolyte of a Lithium–Sulfur Battery During Initial Discharge Using In Situ X-Ray Absorption Spectroscopy Experiments and First-Principles Calculations

Kevin H. Wujcik, Tod A. Pascal, C. D. Pemmaraju, Didier Devaux, Wayne C. Stolte, Nitash P. Balsara, and David Prendergast**

The presence and role of polysulfide radicals in the electrochemical processes of lithium sulfur (Li–S) batteries is currently being debated. Here, first-principles interpretations of measured X-ray absorption spectra (XAS) of Li–S cells are leveraged with an ether-based electrolyte. Unambiguous evidence is found for significant quantities of polysulfide radical species (LiS_3, LiS_4, and LiS_5), including the trisulfur radical anion S_3^-, present after initial discharge to the first discharge plateau, as evidenced by a low energy shoulder in the S K-edge XAS below 2469 eV. This feature is not present in the XAS of cells at increased depth of discharge, which, by our analysis, exhibit increasing concentrations of progressively shorter polysulfide dianions. Through a combination of first-principles molecular dynamics and associated interpretation of in situ XAS of Li–S cells, atomic level insights into the chemistries are provided that underlie the operation and stability of these batteries.

1. Introduction

Despite many years of research, the electrochemical reactions underlying the operation of lithium–sulfur (Li–S) batteries are still the subject of some debate. In particular, the radical trisulfur anion, S_3^-, has concurrently been purported as a key species in the electrochemical process[1–3] or has been discounted as existing in any appreciable concentration during battery operation.[4–6] While one may expect the trisulfur radical to be extremely reactive, there is some reason to believe that it might be stable in solvents commonly used in Li–S batteries. Colorimetric analysis, UV–vis and electron paramagenetic spin resonance (ESR/EPR) spectroscopies have shown that radical anions are stabilized in chemical solutions of polar solvents such as dimethylformamide (DMF)[7–9] and dimethyl sulfoxide (DMSO)[10–12], but not tetrahydrofuran (THF).[9,13] Based on these and similar studies,[14] it is generally accepted that highly polar, electron pair donor solvents such as DMSO and DMF are capable of stabilizing radicals in solutions, while low dielectric constant solvents such as THF cannot.[15] Within the context of Li–S batteries, Barchasz et al. obtained UV–vis and ESR evidence of radical species in an Li–S cell that consisted of poly(ethylene oxide) oligomers with four repeat units (also known as tetraethylene glycol dimethyl ether or TEGDME) mixed with 1 M LiTFSI.[1] Hagen et al. used in situ Raman measurements and theoretical vibrational calculations to show that radical polysulfides are present during cell discharge.[16] More recently, Wang et al. performed in situ ESR on an Li–S cell consisting of a 1,3-dioxolane (DOL), dimethyl ether (DME) (1 M LiTFSI) electrolyte and also detected radicals.[17] In the same study, they also detected the presence of radicals in chemical mixtures of lithium polysulfides in DOL:DME by ESR.

Several questions concerning the presence of radicals during battery operation remain unresolved. This discussion has predominantly focused on the trisulfur radical. While S_3^- could be formed via a direct electrochemical pathway, the prevailing assumption is that it is formed via the dissociation of Li_2S_6 ($Li_2S_6 \rightarrow 2\ LiS_3$).[8,10,12,17] If true, then the redox pathway and voltage profile must significantly depend on the equilibrium constant of the disproportionation reaction, as well as its kinetics. It is also still unclear how critical the formation of polysulfide radical anions is to the remaining redox pathways.[18] It is not known if the radicals are an essential intermediate for complete reduction of sulfur (or complete oxidation of Li_2S). In addition, the concentration of radical anions relative

K. H. Wujcik, Prof. N. P. Balsara
Department of Chemical and Biomolecular Engineering
University of California
Berkeley, CA 94720, USA
E-mail: nbalsara@berkeley.edu
Dr. T. A. Pascal, Dr. C. D. Pemmaraju, Dr. D. Prendergast
The Molecular Foundry
Lawrence Berkeley National Laboratory
Berkeley, CA 94720, USA
E-mail: dgprendergast@lbl.gov
Dr. D. Devaux
Environmental Energy Technologies Division
Lawrence Berkeley National Laboratory
Berkeley, CA 94720, USA
Dr. W. C. Stolte
Advanced Light Source
Lawrence Berkeley National Laboratory
Berkeley, CA 94720, USA

DOI: 10.1002/aenm.201500285

to dilithium sulfide species formed during redox reactions has not been quantified. Questions also emerge regarding the parasitic reactions that take place at the lithium metal anode, and damaging reactions that may take place between radical species and cell electrolytes. The extent to which these effects depend on the choice of solvent/salt electrolyte mixture is also unclear.

As a means of gaining insights into the complex chemistries that underlie Li–S battery systems, X-ray absorption spectroscopy (XAS) has been utilized in several studies.[2,3,5,6,18–22] The attractiveness of XAS is that it is element-specific while also being sensitive to the local bonding chemistry and solvent environment. When properly interpreted, XAS can provide powerful insights into molecular structure and electronic charge state, and, for in situ studies, changes in chemistry due to an external bias. Characterization of the lithium polysulfide species in Li–S batteries usually involves XAS at the sulfur K-edge, i.e., excitations of S 1s core electrons into unoccupied molecular orbitals with local p-character. Recently, Gao et al. investigated the effect of liquid electrolytes on battery performance using S K-edge XAS and found qualitative differences between polar and ethereal solvents during cycling.[3] Cuisinier et al. probed the chemistry of an operational cell by fingerprinting their measured XAS with solid standards.[20] This study clearly demonstrated the production of polysulfide species and lithium sulfide during discharge (due to the consumption of sulfur), although no radicals were invoked in the proposed cathode reaction mechanism. Consistent with these finding, Patel et al. used S K-edge XAS in conjunction with NMR to probe the chemical species formed at the cathode and in the electrolyte during different stages of discharge of the battery, finding that shorter polysulfides were continually being formed at later stages of the discharge.[5] On the other hand, Lowe et al. attempted to uncover the chemistries induced during the discharge process of an Li–S cell with an ether-based solvent (TEGDME) using S K-edge XAS and interpreted their data as providing evidence of the trisulfur radical.[2]

The differences in interpretation of the experimental S K-edge XAS data can be directly traced to reliance on experimentally derived spectral standards coupled with the lack of such standards for polysulfide solutions: due to possible spontaneous polysulfide disproportionation and the establishment of equilibrium mixtures in solution, isolating standards for specific molecular species is necessarily complicated, if not impossible.[6,23] As a result, fingerprinting is frequently performed using solid analogs, which may induce errors in the analysis since the correspondence between the solid and solution phase XAS is by no means guaranteed.[24] This could be an even larger issue for radical anions in solution, since the stabilization and subsequent isolation of the radical is purported to be solvent-dependent, then so might the solution-phase XAS spectral standard. Nevertheless, the solid-state spectral standard of the trisulfur radical anion, measured using crystalline ultramarine samples,[25] has recently been used by Cuisinier et al. to dynamically fingerprint a working Li–S cell.[18] The authors showed that cells containing dimethylacetamide (DMA) (1 M $LiClO_4$) show evidence of LiS_3, while cells containing DOL:DME (1 M $LiClO_4$) do not,[18] which stands in contrast to the ESR findings of Wang et al.[17] It is worth noting that the presence of ESR signals is, perhaps, the most direct signature of the presence of radicals.

A recent advance toward establishing standards, and thus atomistic interpretations of experimental measurements, has been the use of electronic structure methods based on density functional theory (DFT).[21,22,26] Vijayakumar et al. calculated the XAS of the various polysulfides, including the trisulfur radical, in vacuum and in a solvation shell of six DMSO molecules using time-dependent DFT calculations, and used these spectra to fingerprint experimental measurements.[22] In a previous work, we demonstrated that the XAS of dissolved lithium polysulfide dianion species can be obtained via condensed-phase first-principles molecular dynamics and DFT spectral simulations.[21] More recently, we extended our approach to the various polysulfide radicals in vacuum[26] and have predicted that XAS can detect the trisulfur radical against a background of longer chain polysulfide dianions at a ≈20% molar concentration (or ≈4% by spectral composition) at 0.1–0.2 eV spectral resolution. Our condensed phase DFT approach has been proven accurate when compared to measured spectra of known sulfur containing compounds and is extremely insightful for interpreting spectra based on the atomic and electronic properties of the molecule of interest.

In this work, we present, for the first time within the Li–S context, measured X-ray spectra of chemically equilibrated cells at various depths of discharge. Most importantly, we leverage first-principles spectral simulations to deduce the particular sulfur speciation consistent with the measured spectra. We do this using superpositions of our calculated spectra for: the crystalline solid endpoints (S_8 and Li_2S); the intermediate polysulfide dianions (Li_2S_x, where the polysulfide dianion is S_x^{2-}) dissolved in oligomeric PEO; and dissolved radical polysulfide anions (LiS_3, LiS_4, LiS_5), which are the only predicted contributors to low energy absorption features in our S K-edge XAS. Whereas previous studies probed the sulfur cathode in an attempt to directly examine the charge and discharge reaction processes, this present study explores a different question, also pertinent to Li–S cells: if cell discharge were stopped at specific points in the discharge process, what intermediate species would be present in the battery electrolyte after ample time has been given for polysulfide dissolution to occur? This question is of some importance, as real-world consumer batteries will be stopped and started as the user chooses; it would be useful to know what species can be expected in the battery electrolyte if dissolution were to occur. Our results provide further insights into the discharge and disproportionation reactions that take place in the electrolyte during cycling.

2. Results and Discussion

2.1. Experimental XAS of the Li–S Cell at Various Depths of Discharge

We begin our analysis by presenting the schematic for the XAS experiments performed (**Figure 1**a) and an example image of the modified pouch cell (Figure 1b). Li–S cells used in this study comprised cathodes containing elemental sulfur, carbon black, lithium perchlorate ($LiClO_4$), and a diblock copolymer electrolyte polystyrene-poly(ethylene oxide) (SEO). The electrolyte separator consisted of SEO and $LiClO_4$ (r = 0.085). The

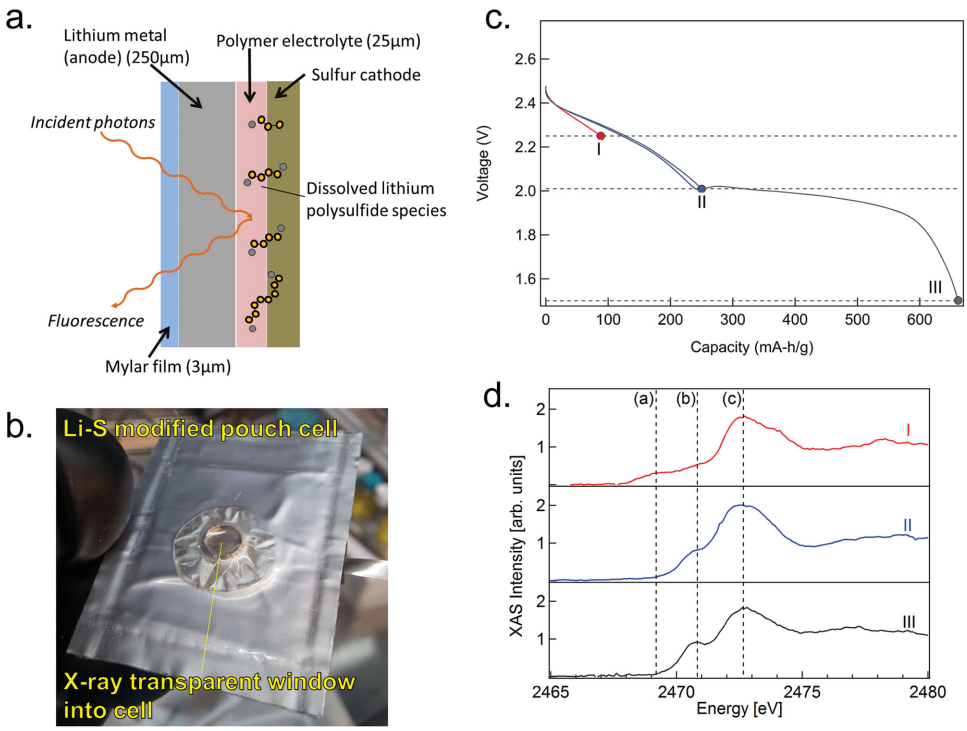

Figure 1. Description of experimental setup and results. a) Schematic of X-ray experiment. b) Diagram of modified Li–S pouch cell. c) *I–V* curves for the three pouch cells tested. The cells were stopped at three different points: I, II, and III, corresponding to 2.25, 2.02, and 1.5 V, respectively. X-ray absorption near-edge structure (XANES) measurements are obtained after holding the cell voltage at the indicated value (dashed horizontal lines) for 3 days. d) Sulfur K-edge XANES as a function of discharge, for each of the three points indicated in (c). Dashed vertical lines are included as a guide to highlight several low energy features below the white line near 2472.6 eV.

anodes were lithium metal foils. Further details are given in the Experimental Section.

We elect to probe through the lithium metal anode side of the battery and into the electrolyte (Figure 1a) in order to maximize the XAS signal of the electrolyte over the cathode. Fresh cells were discharged at a constant current of 41.8 mA g^{-1} (a C/40 discharge rate) at 90 °C using a VMP-3 potentiostat to three specific voltages 2.25, 2.02, and 1.5 V, labeled I, II, and III, respectively. The cell potential versus discharge capacity for the three cells is shown in Figure 1c. After discharging was stopped, cells were then allowed to rest for 3 d at the operating temperature (90 °C), before being probed via XAS at the sulfur K-edge. This procedure means that our measurements are most likely of the equilibrium distributions of polysulfides in the electrolyte. The discharge curves in Figure 1c are qualitatively similar to those reported in the literature.[27] The first-discharge capacity of the fully discharged cell (661 mAh g^{-1}) is less than half of the theoretical capacity of sulfur (1672 mAh g^{-1}). Our objective was not to design a cell to exploit the full capacity of the sulfur cathode, but rather to enable the XAS experiments.

Our measured XAS spectra (Figure 1d) show unique profiles that may point to fundamentally different chemistries. All three spectra have a main feature centered near 2472.6 eV, labeled "c," reminiscent of the sulfur "white-line." Below the main feature is a lower intensity "pre-edge" between 2470.5 and 2471 eV, labeled "b." While this pre-edge feature has been purported as being evidence of the trisulfur radical anion,[2] our previous study revealed the origin to be excitations specific to the terminal S atoms, i.e., those at the end of the polysulfide dianion chains.[21] The intensity and distinctiveness of this feature is found to increase as the cell is discharged. This indicates an increase in the populations of shorter chain polysulfide dianions (i.e. Li_2S_2, Li_2S_3, and Li_2S_4,), as suggested by our previous work[21] and the conclusions of voltage-dependent studies.[1]

Of particular interest, we find that spectrum I, corresponding to a 2.25 V cutoff voltage, exhibits a low energy shoulder in the range 2468–2470 eV, labeled "a," that is below the pre-edge peak "b" at 2470.5–2471 eV. This low energy shoulder is absent in spectra II and III. We note that this feature appears below the pre-edge, suggesting excitations to molecular orbitals of lower energy than the 3p σ^* levels. Some clues to its origin can be found from S K-edge XAS measurements of ultramarine samples. Indeed, Fleet and Liu proposed that the low energy feature near 2468.0 eV from ultramarine powder was due to transitions from the 1s $\rightarrow \pi^*$ (3p) molecular orbital of a radical anion, purported to be trisulfur, trapped in an aluminosilicate cage.[25] Motivated by this study, we calculated the sulfur K-edge XAS spectrum of a lithium trisulfur radical complex (LiS_3) dissolved in TEGDME, an oligomer of PEO comprising four glyme units. The correspondence between the calculated XAS of isolated polysulfide radicals in oligomeric PEO and SEO is inferred from the similar chemical nature and dielectric screening environment of these solvents. These XAS spectra are then used as a basis to fingerprint the XAS of the experimental samples, which undoubtedly contain mixtures of the various species.

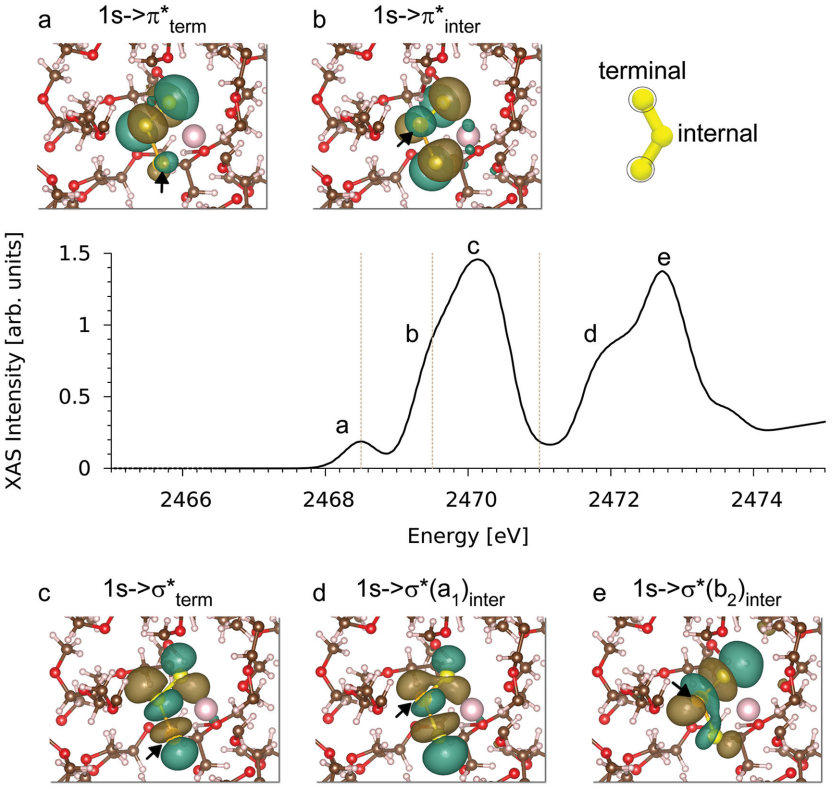

Figure 2. First-principles XANES spectra of the trisulfur LiS_3 molecule dissolved in TEGDME, obtained from sampling ab initio molecular dynamics at 298 K. Each of the five major transitions that inform the spectra is indicated. These can be grouped as excitation from terminal a,c) or internal b,d,e) sulfur atoms (see schematic in upper right). Insets: representative electron density of the resulting excited states. We adopt the convention that the positive phase of the density is colored gold, while the negative phase is colored green. The carbon (gray), oxygen (red), and hydrogen (silver) TEGDME atoms near the LiS_3 molecule are shown. The lithium ion (pink spheres) is also shown. The excited sulfur atom is indicated by the crossed sphere and the arrow.

(1) a low energy peak centered near 2468.5 eV that does indeed arise from 1s→ π* transitions; our analysis indicates that this feature only arises from transitions originating from sulfur 1s core orbitals on either of the two terminal atoms;
(2) a broad, main feature centered near 2470.1 eV with σ* character, which also arises primarily from transitions originating from terminal atoms; we find a low energy shoulder on this main peak, near 2469.5 eV, originating from π* excitations of the internal sulfur atom;
(3) another broad peak near 2472.7 eV that arises from σ* transitions originating from the internal sulfur atom.

In the following analysis, we will focus on spectral contributions to the S K-edge XAS at energies below the white line. Spectral features above this energy for our sulfur-rich samples are undoubtedly affected by overabsorption and perhaps other effects outside the scope of the present study. We note that while the lower energy of the LiS_3 π* compared to the σ* transition is easily understood from standard molecular orbital theory,[26] the 1 eV splitting between the π* transitions originating from the terminal and internal sulfur atoms may appear surprising. In fact, this splitting reflects the increased partial atomic charge around the terminal atoms in the ground state; an effect that reduces the binding energy of their 1s core electrons and thus red-shifts their spectral contribution, reminiscent of the core-level shift effect that informs X-ray photoemission spectroscopy.

We find that the calculated low energy π* peak of the trisulfur radical anion near 2468.5 eV has 1/10th the intensity of the pre-edge feature, due to the delocalized nature of the core-excited π* molecular orbital compared to the σ*. We also note that the π* peak is also not nearly as broad as the pre-edge, due to the lower sensitivity of the π* molecular orbital to bond length variation at finite temperature (with its electron density above and below the molecular plane) than the σ* orbital (which has electron density along the S—S bond). Based on these estimates, we conclude that the relatively weak and narrow π* peak (labeled "a" in **Figure 3**) cannot be the only reason for the observed low energy shoulder (labeled "a" in Figure 2) in sample I.

2.2. Theoretical XAS of Dissolved Lithium Polysulfides

2.2.1. Trisulfur Radical

As noted previously, XAS is an atom specific probe and our computational approach similarly involves combining separate calculations where an S 1s core electron is excited from a single atom. The power of our computational approach is that it facilitates the deconvolution of a spectrum in terms of transitions to specific molecular orbitals, and from particular atoms in a molecule. In the particular case of trisulfur, the first available XAS orbital is the singly occupied π* molecular orbital.[26] In the ground state, this orbital extends over the entire molecule. However, upon absorption of an X-ray photon, the particular core-excited S atom perturbs this orbital, and in different ways depending on its location within the trisulfur chain. We see this by separately considering excitations originating from either the internal (central) sulfur atom or the two terminal atoms. The first-principles-simulated XAS spectrum of a single LiS_3 molecule dissolved in TEGDME is presented in **Figure 2** and can generally be described as having three main features:

2.2.2. Longer-Chain Polysulfide Radicals

In order to explain the origin of the low energy shoulder in the XAS of sample I, we considered longer-chain polysulfide radicals. This was inspired by our previous work, which showed that dissolved polysulfide dianions have slightly longer S—S bond lengths which leads to a red-shift in their XAS peaks.[21]

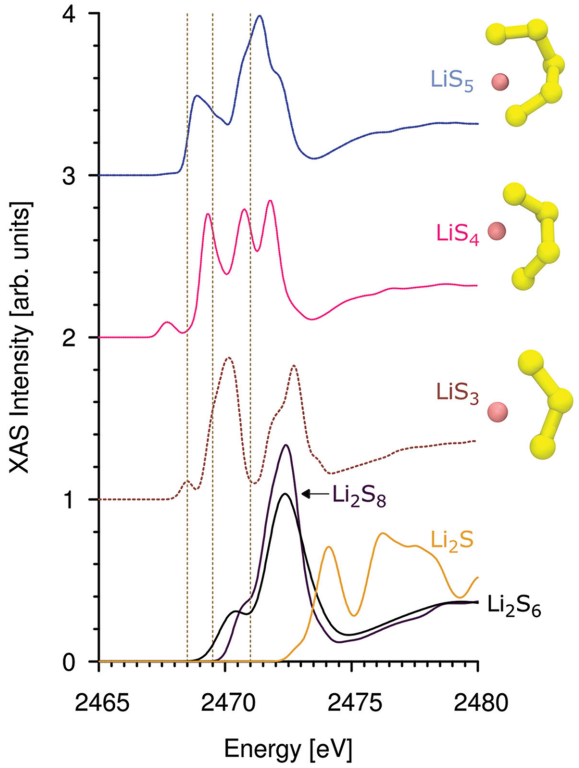

Figure 3. Calculated sulfur K-edge XANES spectra of the solvated radical LiS_5 (blue), LiS_4 (pink), and LiS_3 (brown) molecules. The XANES spectra of the Li_2S_6 (black) and Li_2S_8 (purple) dianions, as well as crystalline Li_2S (gold) from our previous study,[21] are also included. Right outsets: thermodynamically favored state of lithium polysulfide dissolved in TEGDME from AIMD simulations.

To test this hypothesis, we calculated the spectra of LiS_4 and LiS_5 species dissolved in TEGDME. As shown in the inset of Figure 3, the thermodynamically favored geometry of the lithium–radical anion complex in solution is a "claw" structure, with the lithium ion bound to three sulfur atoms, while simultaneously interacting with an oxygen atom on a nearby glyme molecule. In contrast to the three distinct peaks in trisulfur, the XAS of the longer-chain polysulfide radicals are found to be characterized by broader features. In fact, we find that the spectrum of LiS_5 contains only two main features, reminiscent of the spectra of the Li_2S_5 dianion.[21] Therefore, we predict that XAS can distinguish between the LiS_3, LiS_4, and LiS_5 polysulfide radicals. Our simulated XAS of the longer chain radicals [LiS_x; $x = 6, 7, 8$] in vacuum indicate that their spectra are virtually indistinguishable from those of the dianions.[26] Thus, we chose the calculated XAS of the dissolved dianions from our previous work[21] to be representative. This catalog of reference radical anion and dianion spectra from our first-principles calculations then allowed for a semiquantitative fit to experiment.

2.3. Fingerprinting of Measured XAS Using Theory

As already stated, we interpret our XAS measurements using our first-principles spectral standards. Before discussing the results of the fitting procedure, it is important to note the limitations of this approach. First, while the experimental spectra primarily represent the polysulfide species dissolved in the electrolyte separator, it is likely that a minor portion of the incident X-rays was able to pass through the electrolyte (25 μm) and reach the cathode. We have calculated that incident photons have a roughly 18% probability of transmitting through our particular cell, to the cathode, and out to the fluorescence detector. Thus, it is possible that unreacted sulfur in the cathode may manifest itself in the spectra. Second, the obtained spectra are affected by X-ray overabsorption. This causes features at and above the absorption K-edge to be dampened, and features below the edge to effectively appear more intense.[28] While this complication could have been avoided by using a much thinner electrolyte separator (<200 nm), doing so would have resulted in spectra dominated by the cathode. Third, our calculations generally underestimate the oscillator strength of transitions beyond the main edge.[21] Finally, while we present a "best fit" to the experimental spectra, the fit is by no means unique. In fact, other linear combinations provide calculated spectra similar in shape to those shown presently, although they are only slightly different in quantitative composition.

2.3.1. Initial Discharge at 2.25 V

The measured XAS spectrum for cell I and the fitted spectrum are shown in **Figure 4**. The energy scale is divided into four regions labeled A, B, C, and D. Also shown in Figure 4 are the weighted contributions from individual species to the overall spectrum. A visual comparison of the computed LiS_3 spectrum (Figure 3) and the measured spectrum of cell I (Figure 4) indicates that the low energy shoulder cannot be exclusively attributed to LiS_3 as suggested in the literature. In fact, we need to introduce LiS_4 and LiS_5 in order to obtain quantitative agreement between theory and experiment. The apparent presence of these longer chain radical polysulfides is consistent with the ex situ mass spectrometer results of Kawase et al.[29] These three species dominate the low energy shoulder that occupies regions A and B (Figure 4). At energies above 2469 eV contributions from the Li_2S_6 dianion become evident (regions B and C). Introduction of S_8 is essential for obtaining agreement between experiment and theory in region D. The final spectral decomposition of sample I obtained from our least-squares fit (LSF) was 30% contribution from S_8, 25% LiS_5, 22% Li_2S_6 or Li_2S_8, 8% LiS_3, and 16% LiS_4 (**Table 1**). In other words, a linear addition of the theoretical spectra of the pure species listed above with the given weighting results in the dotted curve shown in Figure 4. We also considered other possible contributors to region A (for example, neutral S_3), which do provide a marginally improved fit; however, these species do not appear in our final analysis, since it is not clear how they would be formed during either the electrochemical or disproportionation reactions.

Our analysis indicates that sample I contains a complex mixture of radical anion and dianion sulfur species. Instead of the spectral compositions obtained from our LSF procedure, we could instead consider the corresponding molecular composition, obtained by normalizing with respect to the number

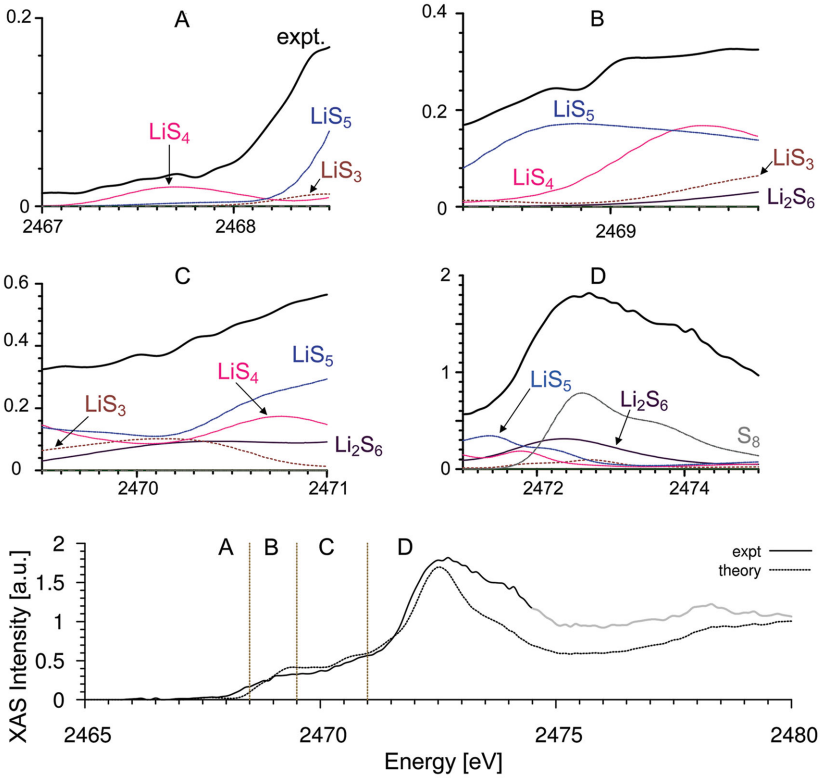

Figure 4. S K-edge XAS during initial stage of discharge (point I in Figure 1). We present a best fit of the experimental data (solid line) using independent spectra obtained from first-principles calculations (dashed line). Due to the likeliness that features above 2474.5 eV stem from radiation damage, fitting is performed below this energy. Four separate regions are identified: region A: features <2469 eV resulting from 1s → π^* transitions of the terminal sulfur atoms on the radical species. Region B: features between 2469 and 2470 eV arising primarily from 1s → σ^* transitions in the terminal atoms of the radical species. Region C: the so-called "pre-edge" between 2470 and 2471.5 eV, arising primarily from 1s → σ^* on the terminal sulfur atoms of the Li_2S_6 dianion and the 1s → π^* transitions on the internal atoms of radicals. Region D: the main edge (including the sulfur white line), resulting primarily from 1s → σ^* excitations of the internal sulfur atoms. Top outsets: zoom of each region, showing the experimental spectra (solid black line) and relative amounts of each of the theoretical spectra in that energy range. The chemical characters of the XANES features are also indicated.

of sulfur atoms in each molecule. The results (**Table 2**) show that the electrolyte contains 17% long chain polysulfide dianions (Li_2S_8 or Li_2S_6), about 62% polysulfide radical anions (LiS_3, LiS_4, and LiS_5), and 20% S_8. We attribute the 20% of the insoluble S_8 present in the spectra to unreacted sulfur in the cathode. The absence of short chain polysulfide dianions (Li_2S_x, x = 2–5) is noteworthy and indicates the long-term stability of the long chain polysulfide dianions.

2.3.2. Subsequent Depths of Discharge

The same approach was used to interpret the measured XAS of samples II and III. Comparisons between theory and experiment are shown in **Figure 5**. Overall, we find that the spectrum of sample II is dominated by short chain polysulfide dianions, as well as a small molecular fraction (≈6%) of the LiS_5 radical anion in order to reproduce the low energy intensity. The main difference between samples I and II is the dramatic decrease in XAS signatures of the LiS_3 and LiS_4 polysulfide radicals, the decreased concentration of unreacted sulfur (to 2%), and for the first time, evidence of significant amounts of solid Li_2S (36%). The decrease in sulfur content may be due to its expected reduction and consumption through electrochemical reactions, or it may also reflect a decrease in X-ray transmittance of the electrolyte due to the increased concentration of dissolved polysulfide species. In summary, short chain dianions dominate the spectra of sample II, with estimated molecular concentrations of 45%, compared to 11% for the long chain dianions.

Finally, we find that the molecular composition of sample III is relatively simple, comprising 61% short chain dianions (23% Li_2S_2, 25% Li_2S_3, 13% Li_2S_5) and 39% Li_2S. It is not clear if the Li_2S detected in our experiments is located within the cathode or the product of side reactions between the lithium metal anode and polysulfides.

2.4. Discharge Mechanism

Some care must be taken when drawing conclusions regarding the sulfur reduction mechanism from the results given above. It is not clear for example, if the species we have identified arise due to electrochemical reactions or from subsequent chemical (disproportionation) reactions. Given the complexity and variety of the species identified in Table 1, it is clear that proposing a unique reaction scheme from these data alone is not possible. The same limitations apply to all previous efforts to determine the sulfur reduction mechanism.[1,2,16,18,20] Nevertheless, we can propose reaction schemes that are consistent with our

Table 1. Exact weights of component spectra used in linear component fits in Figures 3 and 4.

	Voltage [V]	S_8 [%]	Li_2S [%]	LiS_3 [%]	LiS_4 [%]	LiS_5 [%]	Li_2S_2 [%]	Li_2S_3 [%]	Li_2S_5 or Li_2S_4 [%]	Li_2S_6 [%]	Li_2S_8 [%]
I	2.25	30	0	8	16	25	0	0	0	12	10
II	2.02	4	11	0	0	9	0	16	41	20	0
III	1.5	0	17	0	0	0	20	33	30	0	0

Table 2. Molecular composition of samples I, II, and III in terms of six broad families of species: solid S_8 and Li_2S, radicals, short dianions [Li_2S_x; $x = 2–5$] and long dianions [$x = 6, 7, 8$].

	S_8 [%]	Li_2S [%]	Radicals [%]	Dianions (short) [%]	Dianions (long) [%]
I	20	0	62	0	17
II	2	36	6	45	11
III	0	39	0	61	0

data. Such a scheme that accounts for the majority of species detected by our LSF procedure is shown below, and only applies to extremely slow discharge rates.

Step I: Discharging the battery from the original open circuit voltage to 2.25 V, and assuming that elemental sulfur is first converted to Li_2S_8 by reaction (1), the polysulfide radical anions of LiS_3, LiS_4, and LiS_5 are formed by reactions (2a) and (2b).

$$S_8 + 2e^- + 2Li^+ \rightarrow Li_2S_8 \quad (1)$$

$$Li_2S_8 \rightarrow LiS_3 + LiS_5 \quad (2a)$$

$$Li_2S_8 \rightarrow 2LiS_4 \quad (2b)$$

(We assume that the LSF signature of pure sulfur arises because reaction (1) does not go all the way to completion). From reaction (2a), we would expect equal amounts of LiS_3 and LiS_5; however, our molecular composition analysis indicates nearly twice as many molecules of LiS_5, as well as the presence of Li_2S_6. We note that due to the similarity in the XAS, we could not uniquely quantify the amount of Li_2S_6 versus Li_2S_8 (a 1:2 ratio leads to the best fit). Taken together, our results suggest an additional combination reaction of LiS_3 to form Li_2S_6 as given by reaction (3).

$$LiS_3 \rightarrow \frac{1}{2}Li_2S_6 \quad (3)$$

Note that reaction (3) is the reverse of the equilibrium reaction commonly assumed as the origin of the trisulfur radical species in the literature.[8,10,12,17]

Step II: Discharging the battery to 2.02 V, radical anions produced at the cathode in step I are no longer present at this step. This could, in principle, result from either electrochemical consumption or subsequent chemical reactions in the electrolyte. For concreteness, we propose an electrochemical pathway, wherein the radical anions are electrochemically converted into dianions (reactions (4a), (4b), and (4c)), which are reduced subsequently to give Li_2S (reaction (5)).

$$LiS_3 + e^- + Li^+ \rightarrow Li_2S_3 \quad (4a)$$

$$LiS_5 + e^- + Li^+ \rightarrow Li_2S_5 \quad (4b)$$

$$LiS_4 + e^- + Li^+ \rightarrow Li_2S_4 \quad (4c)$$

$$Li_2S_x + 2e^- + 2Li^+ \rightarrow Li_2S + Li_2S_{(x-1)}; 3 \le x \le 5 \quad (5)$$

Based on our LSF analysis, we propose that reactions (4a) and (4c) go to completion, while reaction (4b) does not (i.e. a small amount of LiS_5 is still detected). Similarly, reaction (8) appears not to go to completion, as Li_2S_6 and Li_2S_8 are detected. Due to the similarities in the XAS of Li_2S_5 and Li_2S_4, we are unable to differentiate between these species. It is thus conceivable that

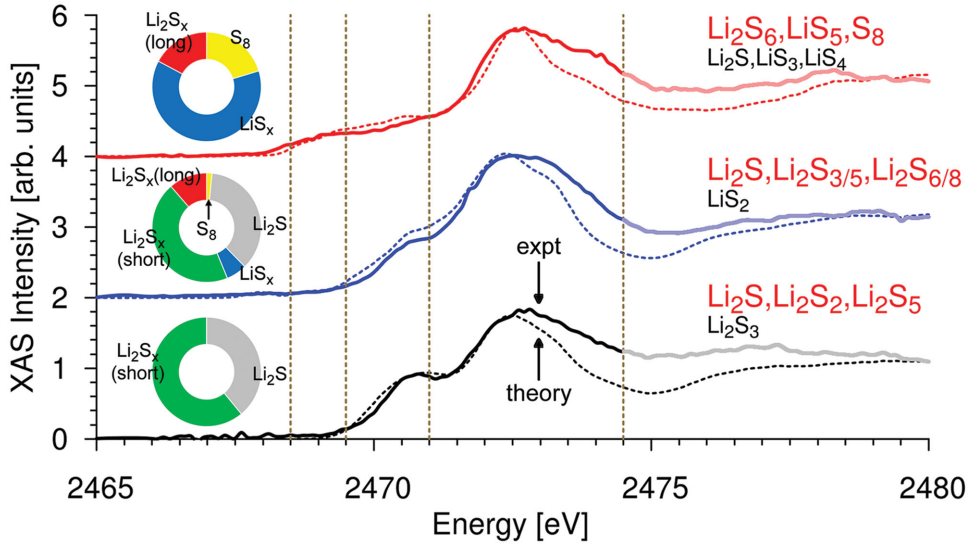

Figure 5. Comparison of the best fit spectra from theory (dashed lines) and XAS measurements (solid lines) for each of the three voltages in Figure 1. The isolated species used to obtain the best fit are also indicated: major components in red, minor components in black. Insets: relative molecular composition ratios of types of sulfur species from our LSF: S_8 (yellow), Li_2S (grey), radicals (blue), and both short (Li_2S_2 to Li_2S_5, green) and long (Li_2S_6/Li_2S_7/Li_2S_8, red) polysulfides dianions.

Li_2S_4 is present in the electrolyte via reaction (4c). Alternatively, the electrochemical consumption of long chain polysulfides by reaction (5) may drive chemical reactions (2a) and (2b) in the reverse direction, thereby reducing radical anion concentrations.

Step III: Discharging the battery to 1.50 V results in significant quantities of short chain polysulfides. This implies that the longer chain polysulfide dianions continue to be converted to Li_2S in the cathode, as described by reaction (6). Presumably, the experimentally measured XAS signal is dominated by polysulfides dissolved in the electrolyte, significantly attenuating the signal from the insoluble Li_2S in the cathode.

$$Li_2S_x + 2e^- + 2Li^+ \rightarrow Li_2S + Li_2S_{(x-1)}; 2 \leq x \leq 5 \quad (6)$$

2.5. Comparison to Previous Work

Finally, we note that in a previous study, we determined species formed by chemical reaction of Li_2S and S_8 in the same electrolyte (poly(ethylene oxide)) used here,[6] with one significant difference now being the presence of lithium perchlorate salt necessary for enabling electrochemical reactions in this study. The main conclusion of our previous work using chemically prepared samples was the proliferation of dissolved lithium polysulfide dianions and the absence of any signal of polysulfide radicals, in contrast to the significant signature of these radicals in the present study in the sample discharged to 2.25 V. Since these chemically prepared samples do not have a source of excess electrons, the electrochemical pathways enumerated above are unavailable and hence the speciation is fundamentally different. This fundamental difference is most clearly exemplified by noting the alternative pathway for the formation of Li_2S_6 during the electrochemical process, i.e., through the recombination of LiS_3 radical anions.

In a recent study, Wang et al. determined the nature of lithium polysulfide species formed in DOL-DME mixtures in both chemically and electrochemically synthesized systems.[17] They used ESR measurements to prove the presence of radical anions in both systems. This is qualitatively different from the present results, obtained in PEO. We note that numerous studies have shown that polysulfide speciation is highly solvent-specific.[7,9,12] Therefore, while illuminating for Li–S electrochemistry in general, the proposed discharge mechanism may prove specific only to solid-state ether-based electrolytes.

3. Conclusions and Outlook

The equilibrium populations of various lithium polysulfide species formed during the discharge of a lithium sulfur battery with an ether-based electrolyte were studied by a combination of theory and experiment. X-ray absorption spectroscopy experiments were conducted on batteries that were discharged to predefined potentials and allowed to rest for 3 days. The experiments were designed to probe the polysulfide species present in the electrolyte as opposed to the transient species formed at the cathode. Spectral fingerprints of S_8 and Li_2S solids, polysulfide dianions, and polysulfide radical anions obtained from first-principles calculations were used to interpret the experimentally measured spectra. It was found that a collection of polysulfide radical anions and long polysulfide dianions dominates the electrolyte composition after the early stage of discharge. As discharge proceeds, the concentration of radical anions decreases and a mixture of short and long chain polysulfide dianions is obtained. At full discharge, the electrolyte contains neither radical anions nor long polysulfide dianions, but solid Li_2S and short polysulfide dianions. A suggested mechanism that is consistent with these findings is then presented. Our use of spectral fingerprints based on first-principles calculations distinguishes this study from previous attempts to determine the mechanism of electrochemical sulfur reductions.

Interpretation of S K-edge XAS on Li–S battery materials is challenging, primarily due to the lack of established standards, but also since the determined populations do not necessarily represent the species formed initially through the active electrochemical process. While some of the observed species may be active role players in the electrochemical process near the electrodes, others may only originate through subsequent disproportionation reactions within the electrolyte. The more explicit importance of our results is that they represent distributions of polysulfide intermediates thermodynamically favored at equilibrium at different points in the discharge curve. In particular, we have shown that radical anions, long deemed unstable in low dielectric solvents, are stable in ether-based electrolytes of a battery at high voltages.

In future work, we intend to explore how the composition of the polysulfide intermediates changes with time after discharge has been stopped. It will be critical to obtain first-principles predictions for the species initially formed electrochemically as well as their thermodynamic and chemical stabilities. Such predictions, when correlated to a time-dependent mapping of measured polysulfide distributions using XAS, will undoubtedely yield important information regarding the kinetics of disproportionation reactions, in particular those that result in the formation of radicals.

4. Experimental Section

Electrolyte Preparation: All electrolyte, cathode, and cell preparation were performed in an argon-filled glovebox (MBraun). Electrolyte films were prepared using a diblock copolymer of polystyrene-poly(ethylene oxide) (SEO) synthesized on a high vacuum line via sequential anionic polymerization, having polystyrene and poly(ethylene oxide) molecular weights of 240 and 269 kg mol^{-1}, respectively, and a polydispersity index (PDI) of 1.26.[30] SEO and dry, battery grade lithium perchlorate ($LiClO_4$) (Sigma-Aldrich) were added to *n*-methylpyrrolidone (NMP) (EMD Millipore) in an amount equivalent to 10 wt% solids, and allowed to mix overnight at 90 °C. The solution was then cast onto nickel foil using a doctor blade and allowed to dry at 60 °C overnight. The resulting film was peeled from the nickel foil and dried under vacuum at 90 °C overnight. The dry film composition had an $LiClO_4$ amount equivalent to an "*r*" value of $r = 0.085$, where "*r*" is the ratio of lithium ions per ethylene oxide monomer.

Cathode Preparation: Cathode slurries contained S_8 (Alfa Aesar), carbon black (Denka), $LiClO_4$, and SEO (identical to that which was used in the electrolyte separator) mixed in NMP, such that the slurry was 15 wt% solids. The slurry

was mixed overnight at 90 °C and subsequently mixed using a homogenizer (Polytron) set to 15 000 RPM. Homogenization was performed three times, 5 min each time with 5 min breaks in between each homogenization to prevent the solution from heating up past undesirable temperatures. The resulting slurry was immediately cast onto electronic grade aluminum foil using a doctor blade and allowed to dry overnight at 50 °C in an argon filled glovebox. The cathode electrode was then dried under vacuum overnight at 50 °C. The dry composition of all cathodes used in the study was 13.0 wt% S_8, 51.4% SEO, 5.5% $LiClO_4$, and 30.1% carbon.

Cell Assembly: Modified pouch cells were prepared by punching a single 3/16 in. hole in the center of one side of aluminum laminate pouch material (Showa Denko). A ring of epoxy was carefully coated around this hole, on the outer side of the pouch, and a 5/8 in. hole of ultrathin 3 µm thick Mylar film (2 spi) was then placed on the top of the epoxy. This was then allowed to dry overnight at room temperature and subsequently dried overnight under vacuum at 90 °C. Pouches were then brought directly into the glovebox without exposure to air.

Circular pieces of cathode and electrolyte were punched from the dried films. Cathode discs were punched to be 7/16 in. in diameter, and electrolyte films, 9/16 in. After punching, thicknesses of cathode and electrolyte discs were measured using a micrometer; mass of cathode discs was measured using a balance (Mettler Toledo). Lithium metal chips (MTI) were used as the anode material and were further punched to be 7/16 in. in diameter. Cathode electrodes were gently pressed to punched electrolyte, placed inside a fluorinated ethylene propylene (FEP) bag and pressed for 30 s using a hand press at room temperature. Lithium metal discs were then pressed to the opposing side of the electrolyte to form a sandwich. The sandwich was then placed in the pouch cell, a nickel tab taped to the lithium metal, and an electronic grade aluminum tab taped to the back of the cathode electrode, using Kapton tape in both cases. Assembled cell pouches were sealed with a vacuum heat sealer (Audionvac). Cells were then annealed overnight at 90 °C to enhance interfacial contact between electrodes and the electrolyte film.

Battery Cycling: Batteries were placed in a temperature-controlled box set to 90 °C and allowed to sit for 12 h before cycling. Cycling was performed using a VMP3 Potentiostat (Bio-Logic). All cells were cycled at a discharge rate corresponding to C/40, calculated using the measured mass of the cathode electrode, the predetermined cathode composition, and assuming a theoretical capacity of 1672 mAh g^{-1} for sulfur. Discharge was stopped at three different voltages: 2.25, 2.02, and the minimum cutoff of 1.50 V. After discharge was stopped, cells were disconnected from potentiostat leads and left to sit at 90 °C for 3 d to allow diffusion of polysulfide species out of the electrolyte.

Experimental X-Ray Absorption Spectroscopy Measurements: XAS measurements were performed at beamline 9.3.1 of the Advanced Light Source (Lawrence Berkeley National Laboratory). Pouch cells were transferred from the glovebox to the beamline endstation chamber, which was kept at ultrahigh vacuum (<6e-7 torr) and at room temperature. Measurements were taken in fluorescence mode using a Hamamatsu silicon photodiode, with 0.1 eV energy resolution around the absorption K-edge. The beam spot size was roughly 5 mm^2. Calibration was performed using sodium thiosulfate (Sigma-Aldrich), setting the first peak maximum to 2472.02 eV. As shown in Figure 1c, incident X-ray photons passed through the anode side of the battery and into the electrolyte. Data were normalized and background subtracted by hand.

5. Theoretical Calculations

Ab initio molecular dynamics (AIMD) simulations: Optimization of the lithium polysulfide species in the gas phase was performed using density functional theory (DFT) calculations employing the Perdew–Burke–Ernzerhof[31] (PBE) generalized-gradient approximation to the exchange-correlation potential. We performed conjugate-gradient minimization of the total energy with respect to the atomic positions using the PWSCF code within the Quantum-ESPRESSO package.[32] The plane-wave pseudopotential calculations used ultrasoft pseudopotentials and a kinetic energy cutoff for electronic wave functions (density) of 25 (200) Ry.

The gas-phase optimized structures were then inserted into the center of a pre-equilibrated box of 24 solvent molecules. By analogy to the poly(ethylene oxide) component of the electrolyte in our samples, we make use of an oligomeric approximation to PEO called tetraethylene glycol dimethyl ether (TEGDME) or tetraglyme. Our AIMD simulations were performed using a modified version of the mixed Gaussian and plane-wave code CP2K/Quickstep.[33] We employed a triple-ζ basis set with two additional sets of polarization functions (TZV2P)[34] and a 320 Ry plane-wave cutoff. The same PBE functional is employed,[31] and the Brillouin zone is sampled at the Γ-point only. Interactions between the valence electrons and the ionic cores are described by norm-conserving pseudopotentials.[35] Solutions to the Poisson equation are provided by an efficient wavelet-based solver.[36] We overcome the poor description of the long-range dispersive forces within the PBE-GGA exchange-correlation functional by employing the DFTD3 empirical corrections of Grimme et al.[37] For each system, we performed at least 50 ps of constant volume constant temperature (NVT) dynamics, saving a snapshot of the system (atomic coordinates and velocities) at every step. The temperature of the system was kept near 300 K using a Nose–Hoover thermostat (temperature damping constant of 100 fs). We allowed for 20 ps of equilibration and 100 snapshots for the system from 20 to 50 ps (evenly spaced every 30 fs) as input to our first-principles X-ray absorption calculations.

First-Principles X-ray absorption spectroscopy calculations: X-ray absorption spectra were calculated within a spin-polarized generalization of the eXcited electron and core hole density functional theory (XCH-DFT) approach.[24] All our XCH calculations employed the same periodic boundary conditions as our AIMD simulations, and used the PBE-GGA functional,[31] and plane-wave ultrasoft pseudopotentials with a kinetic energy cutoff for the electronic wave functions (density) of 25 (200) Ry. Core-excited ultrasoft pseudopotentials and corresponding atomic orbitals were generated with the Vanderbilt code.[38] Matrix elements representing transition amplitude of core excitations were evaluated within the projector-augmented-wave (PAW) frozen-core approximation.[39] The PWSCF code within the Quantum-ESPRESSO package[32] was used to generate the core-excited Kohn–Sham eigenspectrum, while the Shirley interpolation scheme[40] was used to accelerate numerical

convergence of the computed spectra. We include a 0.2 eV Gaussian convolution to guarantee a continuous spectral contribution from each atom. The calculated XAS is taken as the statistical average of the computed spectrum of every sulfur atom in the structure, which further includes intrinsic line shape broadening resulting from finite temperature effects at 298 K.

Least-Squares fitting (LSF): Fitting of the experimental spectra employed the method of least squares using an in-house code. The calculated first-principles XAS of seven dianions [Li_2S_x; x = 2–8], five radical anions [LiS_x; x = 2–6], S_8, and Li_2S were used to construct a hypothetical spectrum that minimized the error in peak positions and intensities when compared to the measured spectrum. Due to concerns of overabsorption and beam damage, the LSF was performed for the energy range spanning from 2465 to 2474.5 eV.

Acknowledgements

K.H.W. and T.A.P. contributed equally to this work. This work was supported by the Assistant Secretary for Energy Efficiency and Renewable Energy, Office of Vehicle Technologies of the US Department of Energy under Contract DE-AC02-05CH11231 under the Batteries for Advanced Transportation Technologies program. Theoretical work was supported by a User Project at The Molecular Foundry and calculations were performed at NERSC, while XAS measurements were made at The Advanced Light Source. The Berkeley Lab User Facilities are supported by the Director, Office of Science, Office of Basic Energy Sciences, of the US Department of Energy under Contract No. DE-AC02-05CH11231.

Received: February 7, 2015
Revised: April 28, 2015
Published online:

[1] C. Barchasz, F. Molton, C. Duboc, J.-C. Leprêtre, S. Patoux, F. Alloin, *Anal. Chem.* **2012**, *84*, 3973.
[2] M. A. Lowe, J. Gao, H. D. Abruna, *RSC Adv.* **2014**, *4*, 18347.
[3] J. Gao, M. A. Lowe, Y. Kiya, H. D. Abruña, *J. Phys. Chem. C* **2011**, *115*, 25132.
[4] L. Nazar, M. Cuisinier, P.-E. Cabelguen, B. Adams, A. Garsuch, M. Balasubramanian, *Energy Environ. Sci.* **2014**, *7*, 2697.
[5] M. U. M. Patel, I. Arčon, G. Aquilanti, L. Stievano, G. Mali, R. Dominko, *Chem. Phys. Chem.* **2014,** *15*, 894.
[6] K. H. Wujcik, J. Velasco-Velez, C. H. Wu, T. Pascal, A. A. Teran, M. A. Marcus, J. Cabana, J. Guo, D. Prendergast, M. Salmeron, N. P. Balsara, *J. Electrochem. Soc.* **2014**, *161*, A1100.
[7] F. Gaillard, E. Levillain, *J. Electroanal. Chem.* **1995**, *398*, 77.
[8] D.-H. Han, B.-S. Kim, S.-J. Choi, Y. Jung, J. Kwak, S.-M. Park, *J. Electrochem. Soc.* **2004**, *151*, E283.
[9] R. D. Rauh, F. S. Shuker, J. M. Marston, S. B. Brummer, *J. Inorg. Nucl. Chem.* **1977**, *39*, 1761.
[10] a) J. Badoz-Lambling, R. Bonnaterre, G. Cauquis, M. Delamar, G. Demange, *Electrochim. Acta* **1976**, *21*, 119; b) R. Bonnaterre, G. Cauquis, *J. Chem. Soc. Chem. Commun.* **1972**, *5*, 293.
[11] B. S. Kim, S. M. Park, *J. Electrochem. Soc.* **1993**, *140*, 115.
[12] R. P. Martin, W. H. Doub, J. L. Roberts, D. T. Sawyer, *Inorg. Chem.* **1973**, *12*, 1921.
[13] S.-I. Tobishima, H. Yamamoto, M. Matsuda, *Electrochim. Acta* **1997**, *42*, 1019.
[14] a) T. Chivers, I. Drummond, *Inorg. Chem.* **1972**, *11*, 2525; b) T. Chivers, P. J. Elder, *Chem. Soc. Rev.* **2013**, *42*, 5996.
[15] a) J. M. Durand, J. OlivierFourcade, J. C. Jumas, M. Womes, C. M. Teodorescu, A. Elafif, J. M. Esteva, R. C. Karnatak, *J. Phys. B. At. Mol. Opt.* **1996**, *29*, 5773; b) V. L. Tauson, J. Goettlicher, A. N. Sapozhnikov, S. Mangold, E. E. Lustenberg, *Eur. J. Mineral.* **2012**, *24*, 133; c) S. Tarling, P. Barnes, J. Klinowski, *Acta Crystallogr. Section B: Struct. Sci.* **1988**, *44*, 128.
[16] M. Hagen, P. Schiffels, M. Hammer, S. Dörfler, J. Tübke, M. J. Hoffmann, H. Althues, S. Kaskel, *J. Electrochem. Soc.* **2013**, *160*, A1205.
[17] Q. Wang, J. Zheng, E. Walter, H. Pan, D. Lv, P. Zuo, H. Chen, Z. D. Deng, B. Y. Liaw, X. Yu, X. Yang, J.-G. Zhang, J. Liu, J. Xiao, *J. Electrochem. Soc.* **2015**, *162*, A474.
[18] M. Cuisinier, C. Hart, M. Balasubramanian, A. Garsuch, L. F. Nazar, *Adv. Energy Mater.* **2015**, DOI: 10.1002/aenm.201401801.
[19] M. Cuisinier, P. E. Cabelguen, B. D. Adams, A. Garsuch, M. Balasubramanian, L. F. Nazar, *Energy Environ. Sci.* **2014**, *7*, 2697.
[20] M. Cuisinier, P.-E. Cabelguen, S. Evers, G. He, M. Kolbeck, A. Garsuch, T. Bolin, M. Balasubramanian, L. F. Nazar, *J. Phys. Chem. Lett.* **2013**, *4*, 3227.
[21] T. A. Pascal, K. H. Wujcik, J. Velasco-Velez, C. Wu, A. A. Teran, M. Kapilashrami, J. Cabana, J. Guo, M. Salmeron, N. Balsara, D. Prendergast, *J. Phys. Chem. Lett.* **2014**, *5*, 1547.
[22] M. Vijayakumar, N. Govind, E. Walter, S. D. Burton, A. Shukla, A. Devaraj, J. Xiao, J. Liu, C. Wang, A. Karim, S. Thevuthasan, *Phys. Chem. Chem. Phys.* **2014**, *16*, 10923.
[23] A. Kamyshny, A. Goifman, J. Gun, D. Rizkov, O. Lev, *Environ. Sci. Technol.* **2004**, *38*, 6633.
[24] D. Prendergast, G. Galli, *Phys. Rev. Lett.* **2006**, *96*, 215502.
[25] M. E. Fleet, X. Liu, *Spectrochim. Acta Part B: At. Spectrosc.* **2010**, *65*, 75.
[26] T. A. Pascal, C. D. Pemmaraju, D. Prendergast, *Phys. Chem. Chem. Phys.* **2015**, *17*, 7743.
[27] a) A. Manthiram, Y. Fu, S.-H. Chung, C. Zu, Y.-S. Su, *Chem. Rev.* **2014**, *114*, 11751; b) A. Manthiram, Y. Fu, Y.-S. Su, *Acc. Chem. Res.* **2012**, *46*, 1125.
[28] a) A. Manceau, K. L. Nagy, *Geochim. Cosmochim. Acta* **2012**, *99*, 206; b) I. J. Pickering, G. N. George, E. Y. Yu, D. C. Brune, C. Tuschak, J. Overmann, J. T. Beatty, R. C. Prince, *Biochemistry* **2001**, *40*, 8138; c) L. Tröger, D. Arvanitis, K. Baberschke, H. Michaelis, U. Grimm, E. Zschech, *Phys. Rev. B: Condens. Matter* **1992**, *46*, 3283.
[29] A. Kawase, S. Shirai, Y. Yamoto, R. Arakawa, T. Takata, *Phys. Chem. Chem. Phys.* **2014**, *16*, 9344.
[30] a) S. A. Mullin, G. M. Stone, A. Panday, N. P. Balsara, *J. Electrochem. Soc.* **2011**, *158*, A619; b) M. Singh, O. Odusanya, G. M. Wilmes, H. B. Eitouni, E. D. Gomez, A. J. Patel, V. L. Chen, M. J. Park, P. Fragouli, H. Iatrou, N. Hadjichristidis, D. Cookson, N. P. Balsara, *Macromolecules* **2007**, *40*, 4578.
[31] J. P. Perdew, K. Burke, M. Ernzerhof, *Phys. Rev. Lett.* **1996**, *77*, 3865.
[32] P. Giannozzi, S. Baroni, N. Bonini, M. Calandra, R. Car, C. Cavazzoni, D. Ceresoli, G. L. Chiarotti, M. Cococcioni, I. Dabo, *J. Phys.: Condens. Matter* **2009**, *21*, 395502.
[33] a) G. Lippert, J. Hutter, M. Parrinello, *Mol. Phys.* **1997**, *92*, 477; b) J. VandeVondele, M. Krack, F. Mohamed, M. Parrinello, T. Chassaing, J. Hutter, *Comput. Phys. Commun.* **2005**, *167*, 103.
[34] J. VandeVondele, J. Hutter, *J. Chem. Phys.* **2007**, *127*, 114105.
[35] a) M. Krack, *Theor. Chem. Acc.* **2005**, *114*, 145; b) S. Goedecker, M. Teter, J. Hutter, *Phys. Rev. B: Condens. Matter* **1996**, *54*, 1703.
[36] L. Genovese, T. Deutsch, S. Goedecker, *J. Chem. Phys.* **2007**, *127*, 054704.
[37] S. Grimme, J. Antony, S. Ehrlich, H. Krieg, *J. Chem. Phys.* **2010**, *132*, 154104.
[38] D. Vanderbilt, *Phys. Rev. B: Condens. Matter* **1990**, *41*, 7892.
[39] G. Kresse, D. Joubert, *Phys. Rev. B: Condens. Matter* **1999**, *59*, 1758.
[40] E. L. Shirley, *Phys. Rev. B: Condens. Matter* **1996**, *54*, 16464.